End-to-End Conformal Calibration for Optimization Under Uncertainty

Christopher Yeh,* Nicolas Christianson,* Alan Wu, Adam Wierman, Yisong Yue
Department of Computing and Mathematical Sciences
California Institute of Technology
Pasadena, CA 91125
{cyeh,nchristi,ywu9,adamw,yyue}@caltech.edu

October 1, 2024

Abstract

Machine learning can significantly improve performance for decision-making under uncertainty in a wide range of domains. However, ensuring robustness guarantees requires well-calibrated uncertainty estimates, which can be difficult to achieve in high-capacity prediction models such as deep neural networks. Moreover, in high-dimensional settings, there may be many valid uncertainty estimates, each with their own performance profile—*i.e.*, not all uncertainty is equally valuable for downstream decision-making. To address this problem, this paper develops an end-to-end framework to *learn* the uncertainty estimates for conditional robust optimization, with robustness and calibration guarantees provided by conformal prediction. In addition, we propose to represent arbitrary convex uncertainty sets with partially input-convex neural networks, which are learned as part of our framework. Our approach consistently improves upon two-stage estimate-then-optimize baselines on concrete applications in energy storage arbitrage and portfolio optimization.

1 Introduction

Well-calibrated estimates of forecast uncertainty are vital for risk-aware decision-making in many real-world systems. For instance, grid-scale battery operators forecast electricity prices to schedule battery charging/discharging to maximize profit, while they rely on uncertainty estimates to minimize financial or operational risk. Similarly, financial investors use forecasts of asset returns along with uncertainty estimates to maximize portfolio returns while minimizing downside risk.

Historically, approaches for decision-making under uncertainty have often treated the estimation of uncertainty separately from its use for downstream decision-making. This "estimate then optimize" (ETO) paradigm [13] separates the problem into an "estimate" stage, where a predictive model is trained to forecast the uncertain quantity, yielding an uncertainty set estimate, followed by an "optimize" stage, where the forecast uncertainty is used to make a decision. Notably, any cost or loss associated with the downstream decision is usually not provided as feedback to the predictive model.

A recent line of work [13, 32, 42, 12] has made steps toward bridging the gap between uncertainty quantification and robust optimization-driven decision-making, where optimization problems take a forecast uncertainty set as a parameter, as is common in energy systems [45, 31] and financial applications [21, 34]. However, existing approaches are suboptimal for several reasons:

1. **The predictive model is not trained with feedback from the downstream objective.** Because the downstream objective is often asymmetric with respect to the forecasting model's error, the trained predictive model, though it provides accurate predictions, may yield significantly worse performance on the true decision-making objective.
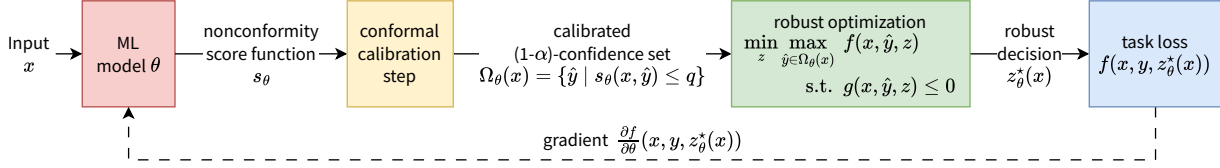
---

*Equal contribution.

Figure 1: Our proposed framework for end-to-end conformal calibration for optimization under uncertainty updates the machine learning model using gradients from the task loss.

2. **For the robust optimization to be tractable, the forecast uncertainty sets have restricted parametric forms.** Common parametric forms include box and ellipsoidal uncertainty sets, limiting the expressivity of uncertainty estimates.

3. **Because neural network models are often poor at estimating their own uncertainty, the forecasts may not be well-calibrated.** Recent approaches such as isotonic regression [24] and conformal prediction [38] have made progress in providing *calibrated* uncertainty estimates from deep learning models, but such methods are typically applied post-hoc to pre-trained models and are therefore difficult to incorporate into an end-to-end training procedure.

As such, there is as of yet *no* comprehensive methodology for training calibrated uncertainty-aware deep learning models end-to-end with downstream decision-making objectives. In this work, we provide the first such methodology. We make three specific contributions corresponding to the three issues identified above:

1. **We develop a methodology for training prediction models end-to-end with downstream decision-making objectives and conformally calibrated uncertainty estimates in the context of the *conditional robust optimization* problem.** This framework is illustrated in Figure 1. By including differentiable conformal calibration layers in our model during training, we close the loop and ensure that feedback from the uncertainty's impact on the downstream objective is accounted for in the training process, since not all model errors nor uncertainty estimates will result in the same downstream cost. This end-to-end training enables the model to focus its learning capacity on minimizing error and uncertainty on outputs with the largest decision-making cost, with more leeway for outputs that have lower costs.

2. **We propose using partially input-convex neural networks (PICNNs) [4] to approximate arbitrary convex uncertainty sets for the conditional robust optimization problem.** Due to the universal convex function approximation property these networks enjoy [11], this approach enables training far more general representations of uncertainty than prior works have considered, which in turn yields substantial improvements on downstream decision-making performance. Importantly, PICNNs are well-matched to our conditional robust optimization problem, as we show that the robust problem resulting from this parametrization can be tractably reformulated as a convex optimization problem.

3. **We propose an exact and computationally efficient method for differentiating through the conformal prediction procedure during training.** In contrast to prior work [40], our method gives exact gradients, without relying on approximate ranking and sorting methods.

Finally, we perform extensive experiments evaluating the performance of our approach on two applications: an energy storage arbitrage task and a portfolio optimization problem. Our code is available on GitHub.[1] We demonstrate conclusively that the combination of end-to-end training with the flexibility of the PICNN-based uncertainty sets consistently improves over ETO baseline methods.

2   Problem Statement and Background

Our problem setting is defined formally as follows: suppose that data $(x, y) \in \mathbb{R}^m \times \mathbb{R}^n$ is sampled i.i.d. from an unknown joint distribution $\mathscr{P}$. Upon observing the input x (but not the label y), an agent makes a decision $z \in \mathbb{R}^p$. After the decision is made, the true label y is revealed, and the agent incurs a *task loss* $f(x, y, z)$, for some known task loss

---

function $f : \mathbb{R}^m \times \mathbb{R}^n \times \mathbb{R}^p \to \mathbb{R}$. In addition, the agent's decision must satisfy a set of joint constraints $g(x, y, z) \leq 0$ coupling x, y, and z.

As an illustrative example, consider an agent who would like to minimize the costs of charging and discharging a battery. The agent may use weather forecasts and historical observations x to predict future energy prices y. Based on the predicted prices, the agent decides on the amount z to charge or discharge the battery. The task loss f is the cost incurred by the agent, and the constraints g include limits on how fast the battery can charge as well as the maximum capacity of the battery. This example is explored in more detail in Section 5.

Because the agent does not observe the label y prior to making its decision, ensuring good performance and constraint satisfaction requires that the agent makes decisions z that are *robust* to the various outcomes of y. A common objective is to choose z to robustly minimize the task loss and satisfy the constraints over all realizations of y within a $(1 - \alpha)$-confidence region $\Omega(x) \subset \mathbb{R}^n$ of the true conditional distribution $\mathscr{P}(y \mid x)$, where $\alpha \in (0, 1)$ is a fixed risk level chosen based on operational requirements. In this case, the agent's robust decision can be expressed as the optimal solution to the following **conditional robust optimization (CRO)** problem [13, 12]:

$$z^\star(x) := \arg\min_{z \in \mathbb{R}^p} \max_{\hat{y} \in \Omega(x)} f(x, \hat{y}, z) \quad \text{s.t.} \quad g(x, \hat{y}, z) \leq 0. \tag{1}$$

After the agent decides $z^\star(x)$, the true label y is revealed, and the agent incurs the task loss $f(x, y, z^\star(x))$. Thus, the agent seeks to minimize the expected task loss

$$\mathbb{E}_{(x,y) \sim \mathscr{P}} \left[f(x, y, z^\star(x)) \right]. \tag{2}$$

While the joint distribution $\mathscr{P}$ is unknown, we assume that we have access to a dataset $D = \{(x_i, y_i)\}_{i=1}^N$ of samples from $\mathscr{P}$. Then, our objective is to train a machine learning model to learn an approximate $(1 - \alpha)$-confidence set $\Omega(x)$ of possible y values for each input x. Formally, our learned $\Omega(x)$ should satisfy the following *marginal coverage* guarantee.

Definition 1 (marginal coverage). An uncertainty set $\Omega(x)$ for the distribution $\mathscr{P}$ provides *marginal coverage at level* $(1 - \alpha)$ if $\mathbb{P}_{(x,y) \sim \mathscr{P}} (y \in \Omega(x)) \geq 1 - \alpha$.

Comparison to related work. The problem of constructing data-driven and machine-learned uncertainty sets with probabilistic coverage guarantees for use in robust optimization has been widely explored in prior literature (*e.g.*, [7, 9, 2, 20]). Chenreddy et al. [13] first coined the phrase "conditional robust optimization" for the problem (1) and considered learning context-dependent uncertainty sets $\Omega(x)$ in this setting, utilizing an approach that integrates clustering with the neural network-parametrized uncertainty representation of Goerigk and Kurtz [20]. Although this uncertainty parametrization is expressive, it results in a mixed integer optimization that is intractable to solve for large-scale problems. Moreover, their approach does not train the uncertainty representation end-to-end based on the task loss, but rather follows the "estimate then optimize" (ETO) paradigm [18], in which the uncertainty set model is trained with a loss agnostic to the eventual downstream task. The lack of feedback from the downstream task loss during training in ETO generally leads to uncertainty sets $\Omega(x)$ which yield suboptimal results. Several other recent papers follow the ETO paradigm using homoskedastic ellipsoidal uncertainty sets [22], heteroskedastic box and ellipsoidal uncertainty sets [41], and a "union of balls" parametrization of uncertainty [32]. In our experiments (see Section 5), we directly compare against the methods proposed by Johnstone and Cox [22] and Sun et al. [41], and we demonstrate consistent improvements over their methods.

Closest to our current work are recent papers [12, 42] which proposed "end-to-end" (E2E) formulations of the CRO problem. Specifically, Chenreddy and Delage [12] poses a training methodology for learning conditional uncertainty sets $\Omega(x)$ for CRO that incorporates a "conditional coverage loss" into the downstream objective, thereby promoting calibrated uncertainty while training $\Omega(x)$ based on the task loss. On the other hand, Wang et al. [42] approaches the end-to-end CRO problem by reformulating the inner maximization problem in their version of (1) into a relaxed form using the Conditional Value-at-Risk (CVaR) and solving for a single uncertainty set Ω that is independent of x. While these papers take significant steps toward learning uncertainty sets end-to-end for conditional robust optimization, they both have substantial limitations. Both papers consider restrictive parametric forms of uncertainty, limiting the performance improvement that their methods can achieve: Chenreddy and Delage [12] focus solely on ellipsoidal uncertainty sets, and Wang et al. [42] restrict to canonical forms of uncertainty sets from the robust optimization

literature such as box, ellipsoidal, and polyhedral uncertainty. In addition, the latter work does not learn x-dependent uncertainty sets, limiting their ability to adapt to heteroscedasticity in $\mathscr{P}(y \mid x)$ and yielding conservative behavior. Moreover, the conditional coverage loss approach in Chenreddy and Delage [12] does not ensure provable coverage guarantees for their learned uncertainty sets, while the CVaR relaxation in Wang et al. [42] will typically yield additional conservativeness.

In contrast, our work avoids these limitations to obtain a more optimal and flexible methodology: we incorporate differentiable conformal calibration layers into our training procedure along with a standard split conformal post-hoc calibration step during inference, which provide provable guarantees on coverage while ensuring that uncertainty is learned end-to-end in a manner that is both calibrated and specifically focused on minimizing the task loss. Furthermore, we propose to use *partially input-convex neural networks* (PICNNs) [4], which provide a general, expressive, and nonparametric representation of conditional convex uncertainty regions that can vary with x and be used efficiently in robust optimization.

Beyond the above closely related work, this paper builds upon and contributes to several different areas in machine learning and robust optimization; see Appendix A for a comprehensive discussion.

3 End-to-End Training of Conformally Calibrated Uncertainty Sets

In this section, we describe our proposed methodological framework for end-to-end task-aware training of predictive models with conformally calibrated uncertainty for the conditional robust optimization problem (1). Figure 1 illustrates our framework, and Algorithm 1 shows pseudocode for both training and inference. Our overarching goal is to learn uncertainty sets $\Omega(x)$ which provide $(1 - \alpha)$ coverage for any choice of $\alpha \in (0, 1)$, and which offer the lowest possible task loss (2).

To this end, we must consider three primary questions:

1. How should the family of uncertainty sets $\Omega(x)$ be parametrized?
2. How can we guarantee that the uncertainty set $\Omega(x)$ provides coverage at level $1 - \alpha$?
3. How can the uncertainty set $\Omega(x)$ be learned to minimize expected task loss?

In this section, we will answer the latter two questions when faced with common parametric forms of the uncertainty set $\Omega(x)$ often used in the literature. Then, in Section 4, we will describe our proposed approach of using PICNNs to represent *general* convex uncertainty sets.

Throughout the rest of the paper, we make the following assumptions on the functions f and g and the uncertainty set Ω in (1) to ensure tractability of the resulting optimization problem.

Assumptions. We assume that the constraint $g(x, y, z) = g(x, z)$ does not depend on y, and that the task loss is of the form $f(x, y, z) = y^\top F z + \tilde{f}(x, z)$ for some matrix $F \in \mathbb{R}^{n \times p}$ and auxiliary function $\tilde{f} : \mathbb{R}^m \times \mathbb{R}^p \to \mathbb{R}$—that is, the task loss decomposes into a function $\tilde{f}(x, z)$ independent of y and a bilinear term $y^\top F z$. We further assume that the functions $g(x, z)$ and $\tilde{f}(x, z)$ are convex in z, and that for each $x \in \mathbb{R}^m$, the uncertainty set $\Omega(x)$ is a convex set.

Note that some of these assumptions can be relaxed under various conditions on the uncertainty set $\Omega(x)$ while maintaining tractability of (1). For example, if $\Omega(x)$ is expressed as the convex hull of a finite set of vertices, then $g(x, y, z)$ can represent a conic constraint (see, *e.g.*, [6, Chapter 6]).

3.1 Conformal uncertainty set calibration

We will consider uncertainty sets represented in the form

$$\Omega_\theta(x) = \{\hat{y} \in \mathbb{R}^n \mid s_\theta(x, \hat{y}) \leq q\}, \tag{3}$$

where $s_\theta : \mathbb{R}^m \times \mathbb{R}^n \to \mathbb{R}$ is an arbitrary *nonconformity score function* that is convex in $\hat{y}$, q is a scalar, and θ collects the parameters of a model that we will seek to learn. Note that this representation loses no generality; *any* family of convex sets $\Omega(x)$ can be represented as such a collection of sublevel sets of a partially input-convex function $s(x, \hat{y})$.

Before we consider how to learn uncertainty sets $\Omega_\theta(x)$ in an end-to-end fashion while ensuring they are calibrated to ensure $(1 - \alpha)$ coverage, we first address the question of how to construct such a calibrated uncertainty set. That is,

---

Algorithm 1 End-to-end conformal calibration for robust decisions under uncertainty

---

    function TRAIN(training data $D = \{(x_i, y_i)\}_{i=1}^{N}$, risk level α, initial model parameters θ)
        for mini-batch $B \subset \{1, \ldots, N\}$ **do**
            Randomly split batch: $B = (B_{\text{cal}}, B_{\text{pred}})$
            Compute threshold $q = \text{QUANTILE}(\{s_\theta(x_i, y_i)\}_{i \in B_{\text{cal}}}, \ 1 - \alpha)$
            for $i \in B_{\text{pred}}$ **do**
                Solve for the robust decision $z_\theta^\star(x_i)$ using (4), (5), or (7)
                Compute gradient of the task loss: $d\theta_i = \partial f(x_i, y_i, z_\theta^\star(x_i))/\partial\theta$
            Update parameters θ using the gradients $\sum_{i \in B_{\text{pred}}} d\theta_i$
    function INFERENCE(model parameters θ, calibration data D_{cal}, risk level α, input x)
        Compute threshold $q = \text{QUANTILE}(\{s_\theta(x_i, y_i)\}_{(x_i, y_i) \in D_{\text{cal}}}, \ 1 - \alpha)$
        return robust decision $z_\theta^\star(x)$ using (4), (5), or (7)
    function QUANTILE(scores $S = \{s_i\}_{i=1}^{M}$, quantile level β)
        $s_{(1)}, \ldots, s_{(M+1)} = \text{SORTASCENDING}(S \cup \{+\infty\})$ ▷ *does not need to be differentiable*
        return $s_{(\lceil (M+1)\beta \rceil)}$

---

given a nonconformity score function $s_\theta(x, \hat{y})$, how should we choose $q \in \mathbb{R}$ to ensure that the uncertainty set $\Omega_\theta(x)$ defined as (3) provides the desired coverage level?

In our work, we use the split conformal prediction procedure [5] at inference time to choose q ensuring that $\Omega_\theta(x)$ provides marginal coverage (Definition 1) at any confidence level $1 - \alpha$. The split conformal procedure assumes access to a calibration dataset $D_{\text{cal}} = \{(x_i, y_i)\}_{i=1}^{M}$ drawn exchangeably from $\mathscr{P}$. We refer readers to Angelopoulos and Bates [5] for details on the split conformal prediction procedure.

Lemma 1 (from Angelopoulos and Bates [5], Appendix D)**.** Let $D_{\text{cal}} = \{(x_i, y_i)\}_{i=1}^{M}$ be a calibration dataset drawn exchangeably (*e.g.*, i.i.d.) from $\mathscr{P}$, and let $s_i = s_\theta(x_i, y_i)$. If $q = \text{QUANTILE}(\{s_i\}_{i=1}^{M}, \ 1 - \alpha)$ (see Algorithm 1) is the empirical $(1 - \alpha)$-quantile of the set $\{s_i\}_{i=1}^{M}$ and (x, y) is drawn exchangeably with D_{cal}, then $\Omega_\theta(x)$ has the coverage guarantee

$$1 - \alpha \leq \mathbb{P}_{x, y, D_{\text{cal}}}(y \in \Omega_\theta(x)) \leq 1 - \alpha + \frac{1}{M+1}.$$

Note that we use split conformal prediction, rather than full conformal prediction, both for computational tractability and to avoid the problem of nonconvex uncertainty sets that can arise from the full conformal approach, as noted in Johnstone and Cox [22]. For the rest of this paper, we assume that $\alpha \in [\frac{1}{M+1}, 1)$ so that $q = \text{QUANTILE}(\{s_i\}_{i=1}^{M}, \ 1 - \alpha) < \infty$ is finite. Thus, for appropriate choices of the nonconformity score function s_θ, the uncertainty set $\Omega_\theta(x)$ is not unbounded.

The split conformal prediction procedure detailed in Lemma 1 gives an approach to selecting $q \in \mathbb{R}$ that ensures the uncertainty set $\Omega_\theta(x)$ satisfies $(1 - \alpha)$ coverage. Note, however, that this process applies to a given nonconformity score function s_θ, and does not address the question of *training* the uncertainty set $\Omega_\theta(x)$ (and hence score function s_θ) to ensure optimal task performance while maintaining coverage. We will propose to apply a separate differentiable conformal prediction procedure during training to address this challenge; we discuss this approach in Section 3.3. First, we will describe in the next section two parametric forms of uncertainty set that are commonly used in the literature.

3.2   Representations of the uncertainty set

In this section, we briefly describe two standard uncertainty set representations, box and ellipsoidal uncertainty, which yield tractable forms of the robust optimization problem (1). In both cases, the uncertainty set has the form $\Omega_\theta(x) = \{\hat{y} \in \mathbb{R}^n \mid s_\theta(x, \hat{y}) \leq q\}$ for some function $s_\theta : \mathbb{R}^m \times \mathbb{R}^n \to \mathbb{R}$, and thus matches the form (3) in Section 3.1 that enables conformal calibration. Then, in Section 3.3, we discuss how to train predictive models to generate these uncertainty sets end-to-end within a robust optimization framework.

Box uncertainty sets.   One of the simplest representations of uncertainty is box uncertainty where $\Omega(x) = [\underline{y}(x), \overline{y}(x)]$ is an n-dimensional box whose lower and upper bounds depend on x. The particular parametrization we use takes inspiration from quantile regression in the univariate setting. Let $h_\theta : \mathbb{R}^m \to \mathbb{R}^n \times \mathbb{R}^n$ be a neural network that estimates

lower and upper bounds: $h_\theta(x) = (h_\theta^{\text{lo}}(x), h_\theta^{\text{hi}}(x))$. To represent a box uncertainty set in the form (3), we define a nonconformity score function as a generalization of that from scalar conformalized quantile regression [37]:

$$s_\theta(x,y) = \max \cup_{i=1}^{n} \left\{ h_\theta^{\text{lo}}(x)_i - y_i, \ y_i - h_\theta^{\text{hi}}(x)_i \right\}.$$

Then, the uncertainty set (3) becomes

$$\Omega_\theta(x) = \{\hat{y} \in \mathbb{R}^n \mid s_\theta(x,\hat{y}) \le q\} = \left[h_\theta^{\text{lo}}(x) - q\mathbf{1}, \ h_\theta^{\text{hi}}(x) + q\mathbf{1}\right] =: \left[\underline{y}(x), \ \overline{y}(x)\right],$$

which is calibrated when q is chosen by the split conformal procedure detailed in Section 3.1.

Given a box uncertainty set $\Omega_\theta(x)$, it is possible to take the dual of the inner maximization problem (see Appendix B.1) to transform the robust optimization problem (1) into an equivalent tractable form:

$$z_\theta^\star(x) = \operatorname*{arg\,min}_{z \in \mathbb{R}^p} \min_{\nu \in \mathbb{R}^n} \ \left(\overline{y}(x) - \underline{y}(x)\right)^\top \nu + \underline{y}(x)^\top Fz + \tilde{f}(x,z)$$
$$\text{s.t.} \quad \nu \ge \mathbf{0}, \quad \nu - Fz \ge \mathbf{0}, \quad g(x,z) \le 0. \tag{4}$$

This problem is convex, and hence tractable, so long as $\tilde{f}(x,z)$ and $g(x,z)$ are convex in z.

Ellipsoidal uncertainty sets. Another common form of uncertainty set is that of ellipsoidal uncertainty. Suppose a neural network model outputs predicted mean and covariance parameters $h_\theta(x) = (\mu_\theta(x), \Sigma_\theta(x))$ of a multivariate normal distribution, so that we have a predicted conditional density $\hat{\mathscr{P}}(y \mid x; \theta) = \mathscr{N}(y \mid \mu_\theta(x), \Sigma_\theta(x))$, where $\mathscr{N}(\cdot \mid \mu, \Sigma)$ is the multivariate normal density function. In this case, we define the nonconformity score function based on the squared Mahalanobis distance [22, 41]

$$s_\theta(x,y) = (y - \mu_\theta(x))^\top (\Sigma_\theta(x))^{-1} (y - \mu_\theta(x)),$$

which yields uncertainty sets (3) that are ellipsoidal:

$$\Omega_\theta(x) = \{\hat{y} \in \mathbb{R}^n \mid s_\theta(x,\hat{y}) \le q\} = \{\hat{y} \in \mathbb{R}^n \mid (\hat{y} - \mu_\theta(x))^\top (\Sigma_\theta(x))^{-1} (\hat{y} - \mu_\theta(x)) \le q\},$$

which is calibrated when q is chosen by the split conformal procedure detailed in Section 3.1. By taking the dual of the inner maximization problem and invoking strong duality (see Appendix B.2), it is possible to transform the robust optimization problem (1) into the equivalent tractable form:

$$z_\theta^\star(x) = \operatorname*{arg\,min}_{z \in \mathbb{R}^p} \ \sqrt{q} \cdot \|(\Sigma_\theta(x))^{1/2} Fz\|_2 + \mu_\theta(x)^\top Fz + \tilde{f}(x,z)$$
$$\text{s.t.} \quad g(x,z) \le 0, \tag{5}$$

which is convex, and hence tractable, so long as $\tilde{f}(x,z)$ and $g(x,z)$ are convex in z.

3.3 End-to-end training and calibration

Thus far, we have discussed how to calibrate an uncertainty set $\Omega_\theta(x)$ of the form (3) to ensure coverage, and we described two choices of score function s_θ parametrizing common box and ellipsoidal uncertainty sets. However, to ensure that the uncertainty sets $\Omega_\theta(x)$ *both* guarantee coverage *and* ensure optimal downstream task performance, it is necessary to design an end-to-end training methodology that can incorporate both of these desiderata in a fully differentiable manner. We propose such a methodology in Algorithm 1.

Our end-to-end training approach uses minibatch gradient descent to minimize the empirical task loss $\ell(\theta) = \frac{1}{N}\ell_i(\theta)$ where $\ell_i(\theta) = f(x_i, y_i, z_\theta^\star(x_i))$. This requires differentiating through both the robust optimization problem as well as the conformal prediction step. The gradient of the task loss on a single instance is $\frac{d\ell_i}{d\theta} = \frac{\partial f}{\partial z}\big|_{(x_i, y_i, z_\theta^\star(x_i))} \frac{\partial z_\theta^\star}{\partial \theta}\big|_{x_i}$, where $\frac{\partial z_\theta^\star}{\partial \theta}\big|_{x_i}$ can be computed by differentiating through the Karush–Kuhn–Tucker (KKT) conditions of the convex reformulation of the optimization problem (1) (*i.e.*, the problems (4), (5)) following the approach of Amos and Kolter [3], under mild

6

assumptions on the differentiability of f and g. Note that the gradient of any convex optimization problem can be computed with respect to its parameters as such [1, Appendix B].

To include calibration during training, we assume that for every (x,y) in our training set, $s_\theta(x,y)$ is differentiable w.r.t. θ almost everywhere; this assumption holds for common nonconformity score functions, including those used in this paper. We then adopt the conformal training approach [40] in which a separate q is chosen in each minibatch, as shown in Algorithm 1. The chosen q depends on θ (through s_θ), and $z_\theta^\star(x_i)$ depends on the chosen q. Therefore $\frac{\partial z_\theta^\star}{\partial \theta}$ involves calculating $\frac{\partial z_\theta^\star}{\partial q}\frac{\partial q}{\partial \theta}$, where $\frac{\partial q}{\partial \theta}$ requires differentiating through the empirical quantile function. Whereas Stutz et al. [40] uses a smoothed approximate quantile function for calculating q, we find the smoothing unnecessary, as the gradient of the empirical quantile function is unique and well-defined almost everywhere. Importantly, our exact gradient is both more computationally efficient and simpler to implement than the smoothed approximate quantile approach. We describe our approach in greater detail in Appendix C.

After training has concluded and we have performed the final conformal calibration step, the resulting model enjoys the following theoretical guarantee on performance (*cf.* [41, Proposition 1]).

Proposition 1. After following our training and calibration procedure, we achieve with probability $1 - \alpha$ (with respect to x, y, and the calibration set D_{cal}) the following upper bound on task loss:

$$f(x, y, z_\theta^\star(x)) \le \min_{z \in \mathbb{R}^p} \max_{\hat{y} \in \Omega_\theta(x)} f(x, \hat{y}, z) \qquad \text{s.t.} \qquad g(x, \hat{y}, z) \le 0.$$

This result is an immediate consequence of the split conformal coverage guarantee from Lemma 1, which ensures that for the true $(x,y) \sim \mathscr{P}$, $\mathbb{P}_{x,y,D_{\text{cal}}}(y \in \Omega_\theta(x)) \ge 1 - \alpha$. The realized task loss will therefore, with probability $1 - \alpha$, improve on the optimal value of the robust problem (1). Moreover, this guarantee holds despite the fact that the distribution $\mathscr{P}(y \mid x)$ is unknown, and the dependence of the learned uncertainty set $\Omega_\theta(x)$ on x allows for taking advantage of heteroskedasticity that, together with our end-to-end training framework, yield substantial improvements in average-case performance in conjunction with our the robust guarantee offered by Proposition 1.

4 Representing General Convex Uncertainty Sets via PICNNs

In the previous section, we discussed how to calibrate a generic family of uncertainty sets $\Omega_\theta(x)$ expressed as the sublevel sets of a nonconformity score function as in (3); we then described an end-to-end training methodology for learning such calibrated uncertainty sets to optimize downstream task loss. However, both box and ellipsoidal uncertainty sets are highly restrictive representations of uncertainty whose particular shapes may yield suboptimal task loss performance. If we could instead let $\Omega_\theta(x)$ range over the set of *all* convex uncertainty sets, this more expressive class would enable obtaining better task loss.

To this end, we propose to directly learn a partially-convex nonconformity score function $s_\theta : \mathbb{R}^m \times \mathbb{R}^n \to \mathbb{R}$ that is convex only in the second input vector. Fixing x, any q-sublevel set $\{\hat{y} \in \mathbb{R}^n \mid s_\theta(x, \hat{y}) \le q\}$ of s_θ is a convex set, and likewise every family of convex sets can be expressed as the q-sublevel sets of some partially-convex function. To implement this approach, we are faced with two questions:

1. How should we parametrize the score function s_θ to allow $\Omega_\theta(x)$ to approximate *arbitrary* convex uncertainty sets?
2. Does the chosen uncertainty set representation yield a tractable convex reformulation of the CRO problem (1)?

A natural answer to the first question is to use a partially input-convex neural network (PICNN) [4] as s_θ; these can efficiently approximate any partially-convex function [11]. We consider a PICNN defined as $s_\theta(x,y) = W_L \sigma_L + V_L y + b_L$, where

$$\sigma_0 = \mathbf{0}, \qquad u_0 = x \qquad\qquad W_l = \bar{W}_l \operatorname{diag}([\hat{W}_l u_l + w_l]_+) \tag{6a}$$
$$u_{l+1} = \operatorname{ReLU}(R_l u_l + r_l) \qquad\qquad V_l = \bar{V}_l \operatorname{diag}(\hat{V}_l u_l + v_l) \tag{6b}$$
$$\sigma_{l+1} = \operatorname{ReLU}(W_l \sigma_l + V_l y + b_l) \qquad\qquad b_l = \bar{B}_l u_l + \bar{b}_l. \tag{6c}$$

The weights of the neural network are $\theta = (R_l, r_l, \bar{W}_l, \hat{W}_l, w_l, \bar{V}_l, \hat{V}_l, v_l, \bar{B}_l, \bar{b}_l)_{l=0}^{L}$, and the matrices $\bar{W}_l$ are constrained to be entrywise nonnegative to ensure convexity of s_θ with respect to y. For ease of notation, we assume all hidden layers $\sigma_1, \ldots, \sigma_L$ have the same dimension d.

We are now faced with the second question above: does the PICNN representation of the uncertainty set $\Omega_\theta(x)$ allow for a tractable reformulation of the CRO problem (1)? Fortunately, as we show in the following theorem, the answer is yes.

Theorem 1. Let $\Omega_\theta(x) = \{\hat{y} \in \mathbb{R}^n \mid s_\theta(x, \hat{y}) \leq q\}$, where s_θ is a PICNN as defined in (6). Then the CRO problem (1) with uncertainty set $\Omega_\theta(x)$ is equivalent to the following tractable minimization problem:

$$
\begin{aligned}
z_\theta^\star(x) = \arg\min_{z \in \mathbb{R}^p} \min_{\nu \in \mathbb{R}^{2Ld+1}} \quad & b(\theta, q)^\top \nu + \tilde{f}(x, z) \\
\text{s.t.} \quad & A(\theta)^\top \nu = \begin{bmatrix} Fz \\ \mathbf{0} \end{bmatrix}, \quad \nu \geq \mathbf{0}, \quad g(x, z) \leq 0
\end{aligned}
\tag{7}
$$

where $A(\theta) \in \mathbb{R}^{(2Ld+1) \times (n+Ld)}$ and $b(\theta, q) \in \mathbb{R}^{2Ld+1}$ are constructed from the weights θ of the PICNN (6), and b also depends on q. Note that if $\tilde{f}(x, z)$ and $g(x, z)$ are convex in z, then (7) is convex, and hence tractable.

We prove Theorem 1 in Appendix B.3; the main idea is that when $\Omega_\theta(x)$ is a sublevel set of a PICNN, we can equivalently reformulate the inner maximization problem in (1) as a linear program, which allows taking the dual of the inner problem to yield a tractable minimization problem.

Since the PICNN uncertainty sets are of the same form as (3) and they yield the tractable convex reformulation (7) of the CRO problem (1), we can apply the same split conformal procedure detailed in Section 3.1 to choose $q \in \mathbb{R}$ and obtain coverage guarantees on $\Omega_\theta(x)$, and we can employ the same end-to-end training methodology proposed in Section 3.3 to train calibrated uncertainties end-to-end using the downstream task loss. Note that in some cases during training, the inner maximization problem of (1) with PICNN-parametrized uncertainty set may be unbounded (if $\Omega_\theta(x)$ is not compact) or infeasible (if too small a q was chosen by the split conformal procedure and $\Omega_\theta(x)$ is empty). This will lead, respectively, to an infeasible or unbounded equivalent problem (7). We can avoid this concern by slightly adjusting the PICNN architecture to ensure its sublevel sets are compact and by suitably increasing q when needed to ensure $\Omega_\theta(x)$ is never empty. Such modifications do not change the general form of the problem (7) and preserve the marginal coverage guarantee for the uncertainty set $\Omega(x)$; see Appendix B.4 for details.

5 Experiments

5.1 Problem descriptions

We consider two applications in our experiments: price forecasting for battery storage operation, and a portfolio optimization task.

Price forecasting for battery storage. This problem comes from Donti et al. [15], where a grid-scale battery operator predicts electricity prices $y \in \mathbb{R}^T$ over a T-step horizon and uses the predicted prices to decide on a battery charge/discharge schedule for price arbitrage. The input features x include the past day's prices and temperature, the next day's energy load forecast and temperature forecast, binary indicators of weekends or holidays, and yearly sinusoidal features. The operator decides how much to charge ($z^{\text{in}} \in \mathbb{R}^T$) or discharge ($z^{\text{out}} \in \mathbb{R}^T$) the battery, which changes the battery's state of charge ($z^{\text{state}} \in \mathbb{R}^T$). The battery has capacity B, charging efficiency γ, and maximum charging/discharging rates c^{in} and c^{out}. The task loss function represents the multiple objectives of maximizing profit, flexibility to participate in other markets by keeping the battery near half its capacity (with weight λ), and battery health by discouraging rapid charging/discharging (with weight ε):

$$
f(y, z) = \sum_{t=1}^{T} y_t (z^{\text{in}} - z^{\text{out}})_t + \lambda \left\| z^{\text{state}} - \frac{B}{2} \mathbf{1} \right\|^2 + \varepsilon \left\| z^{\text{in}} \right\|^2 + \varepsilon \left\| z^{\text{out}} \right\|^2.
$$

The constraints are given by

$$z_0^{\text{state}} = B/2, \qquad z_t^{\text{state}} = z_{t-1}^{\text{state}} - z_t^{\text{out}} + \gamma z_t^{\text{in}} \qquad \forall t = 1, \ldots, T$$
$$0 \le z^{\text{in}} \le c^{\text{in}}, \qquad 0 \le z^{\text{out}} \le c^{\text{out}}, \qquad 0 \le z^{\text{state}} \le B.$$

Following Donti et al. [15], we set $T = 24$ hours, $B = 1$, $\gamma = 0.9$, $c^{\text{in}} = 0.5$, $c^{\text{out}} = 0.2$, $\lambda = 0.1$, and $\varepsilon = 0.05$.

Portfolio optimization We adopt the portfolio optimization setting from Chenreddy and Delage [12], where the prediction targets $y \in \mathbb{R}^n$ are the returns of a set of n securities, and the decision variables $z \in \mathbb{R}^n$ are the portfolio weights. The task loss is $f(y, z) = -y^\top z$, and the constraints are given by $0 \le z$, $\mathbf{1}^\top z = 1$.

Following the experimental setup in Chenreddy and Delage [12], we consider a synthetic dataset where $(x, y) \in \mathbb{R}^{2 \times 2}$ are drawn from a mixture of three 4-D multivariate normal distributions. Due to space constraints, we provide more data details in Appendix D.2 and report experimental results in Appendix D.3.

5.2 Baseline methods

We implemented several "estimate-then-optimize" (ETO) baselines, listed below, to compare against our end-to-end (E2E) method. These two-stage ETO baselines are trained using task-agnostic losses such as pinball loss or negative log-likelihood, with conformal calibration applied after training to satisfy marginal coverage and ensure fair comparison against our E2E method.

- ETO denotes models that have identical neural network architectures to our E2E models, differing only in the loss function during training. The box uncertainty ETO model is trained with pinball loss to predict the $\alpha/2$ and $1 - \alpha/2$ quantiles. The ellipsoidal uncertainty ETO model predicts a mean vector and covariance matrix and is trained with a multivariate normal negative log-likelihood loss. For the PICNN ETO model, we give probabilistic interpretation to a PICNN model s_θ via the energy-based model $\hat{\mathscr{P}}(y \mid x) \propto \exp(-s_\theta(x, y))$ and train it using the negative log-likelihood (NLL) loss function $\text{NLL}(s_\theta(x, y)) = \ln s_\theta(x, y) + \ln Z_\theta(x)$, where $Z_\theta(x) = \int_{y \in \mathbb{R}^n} \exp(-s_\theta(x, y)) \, \mathrm{d}y$, following the approach of Lin and Ba [26]. More details of the ETO models are given in Appendix D.
- ETO-SLL denotes our implementation of the box and ellipsoid uncertainty ETO methods from Sun et al. [41]. Unlike our ETO models, ETO-SLL first trains a point estimate model (without uncertainty) with mean-squared error loss. Then, ETO-SLL box and ellipsoidal uncertainty sets are derived from training a separate quantile regressor using pinball loss to predict the $(1 - \alpha)$-quantiles of absolute residuals or ℓ_2-norm of residuals of the point estimate. Unlike ETO which can learn ellipsoidal uncertainty sets with different covariance matrices for each input x, the ETO-SLL ellipsoidal uncertainty sets all share the same covariance matrix (scaled differently for each x).
- ETO-JC denotes our implementation of the ETO method by Johnstone and Cox [22], which only applies to ellipsoid uncertainty. Like ETO-SLL, ETO-JC also first trains a point estimate model (without uncertainty) with mean-squared error loss. ETO-JC uses the same covariance matrix (with the same scale) for each input x.

5.3 Experimental results: Battery storage problem

Figure 2 compares task loss performance for different uncertainty levels ($\alpha \in \{.01, .05, .1, .2\}$) and the different uncertainty set representations for both the ETO baselines and our proposed E2E methodology when deployed on the battery storage problem with no distribution shift. We find that our E2E approach consistently yields improved performance over all ETO baslines, for all three uncertainty set parameterizations, and over all tested uncertainty levels α. Moreover, the PICNN uncertainty representation, when trained end-to-end, improves on the performance offered by both box and ellipsoidal uncertainty at all uncertainty levels. We additionally show the corresponding coverage obtained by the learned uncertainty sets in Figure 3; all the models and training methodologies obtain coverage close to the target level, confirming that the improvements in task loss performance from our E2E approach do not come at the cost of worse coverage.

5.4 Performance under distribution shift

The aforementioned results were produced without distribution shift, where our training and test sets were sampled uniformly at random, thus ensuring exchangeability and guaranteeing marginal coverage. In this section, we evaluate
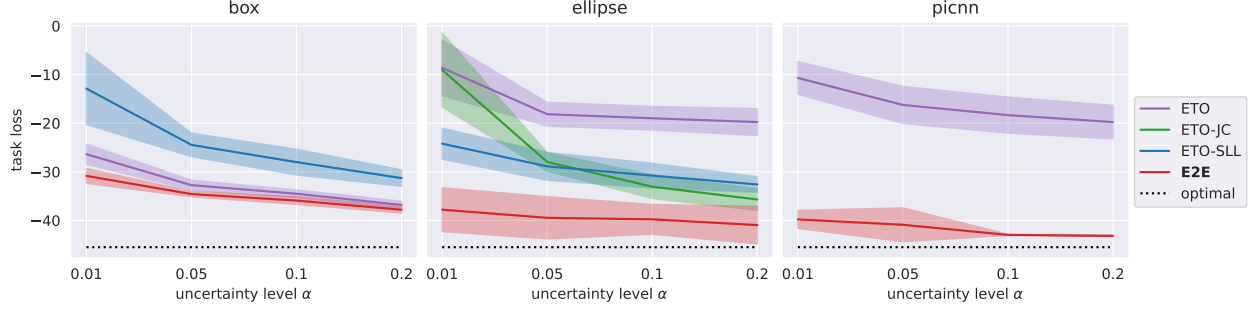
Figure 2: Task loss performance (mean ± 1 stddev across 10 runs) for the battery storage problem with no distribution shift. Lower values are better.
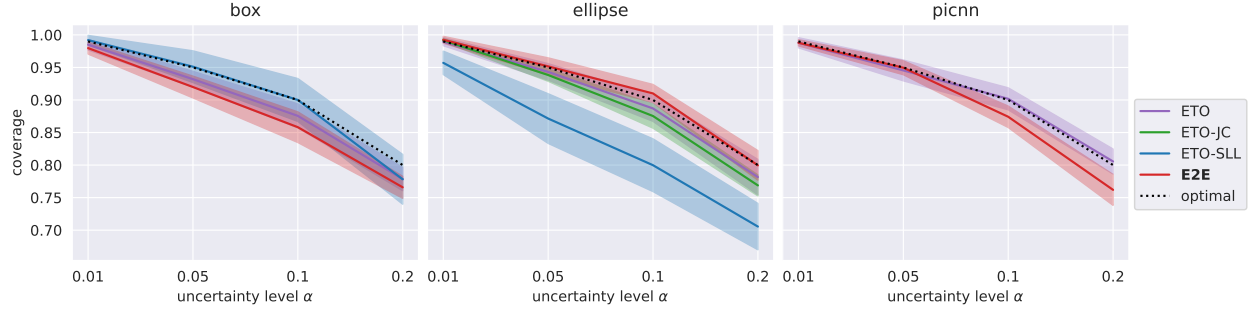

Figure 3: Coverage (mean ± 1 stddev across 10 runs) for the battery storage problem with no distribution shift, with the dotted black line indicating the target coverage level $1 - \alpha$.

our method on the more realistic setting with distribution shift by splitting our data temporally; our models are trained on the first 80% of days and evaluated on the last 20% of days. Figures 4 and 5 mirror Figures 2 and 5, except that there is now distribution shift. We again find that our E2E approach consistently yields improved performance over all ETO baselines, for all three uncertainty set parameterizations, and for all tested uncertainty levels α. Moreover, both the ellipsoidal and PICNN uncertainty representations, when trained end-to-end, improve on the performance offered by box uncertainty, with PICNN and ellipsoidal uncertainty performing comparably. In terms of coverage (Figure 5), we find that under distribution shift, the models do not provide the same level of coverage guaranteed in the i.i.d. case, and the ellipsoidal and PICNN models tend to provide worse coverage than the box uncertainty. This is not too surprising, however, since these two models offer greater representational power, and thus might be fitting too closely to the pre-shift distribution, which impacts robustness under distribution shift. Devising methods to anticipate distribution shift when training these more expressive models, and in particular the PICNN-based uncertainty, remains an interesting avenue for future work.

6   Conclusion

In this work, we develop the first end-to-end methodology for training predictive models with uncertainty estimates (with calibration enforced differentiably throughout training) that are utilized in downstream conditional robust optimization problems. We propose an approach utilizing partially input-convex neural networks (PICNNs) to represent general convex uncertainty regions, and we perform extensive experiments on a battery storage application and a portfolio optimization task, which validate the utility of our end-to-end approach and the expressiveness of the PICNN representation.

Limitations   Our framework requires various assumptions on the functions f and g in the conditional robust optimization problem (1) in order to ensure tractability, such as convexity and bilinearity in (y, z). In addition, while the
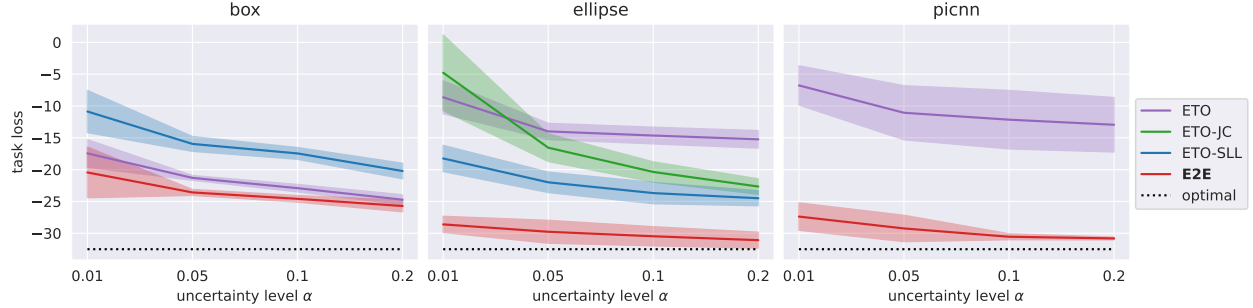
Figure 4: Task loss performance (mean ± 1 stddev across 10 runs) for the battery storage problem with distribution shift. Lower values are better.
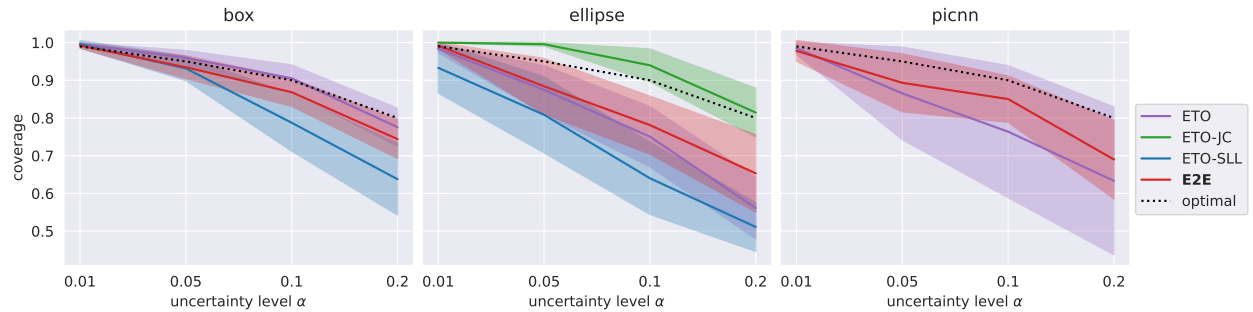

Figure 5: Coverage (mean ± 1 stddev across 10 runs) for the battery storage problem with distribution shift, with the dotted black line indicating the target coverage level $1 - \alpha$.

PICNN uncertainty representation can represent general convex uncertainties, it cannot handle more general nonconvex uncertainty regions. Removing these assumptions and approaching more general stochastic and robust optimization problems using, *e.g.*, policy gradient methods would be an interesting direction for future work.

Broader Impacts Our work, which introduces a methodology to improve the performance and robustness for a class of robust optimization problems, has the potential for positive societal impact via deployment to problems such as battery storage operation, where better decisions in the face of uncertainty can help with grid-scale decarbonization efforts. Due to the primarily methodological contributions of this work, we do not anticipate negative societal impacts or the need for safeguards.

Acknowledgments

References

[1] A. Agrawal, B. Amos, S. Barratt, S. Boyd, S. Diamond, and J. Z. Kolter. Differentiable Convex Optimization Layers. In *Advances in Neural Information Processing Systems*, volume 32. Curran Associates, Inc., 2019. URL https://papers.nips.cc/paper_files/paper/2019/hash/9ce3c52fc54362e22053399d3181c638-Abstract.html.

[2] P. Alexeenko and E. Bitar. Nonparametric Estimation of Uncertainty Sets for Robust Optimization. In *2020*

59th IEEE Conference on Decision and Control (CDC), pages 1196–1203, Jeju, Korea (South), Dec. 2020. IEEE. ISBN 978-1-72817-447-1. doi: 10.1109/CDC42340.2020.9303863. URL https://ieeexplore.ieee.org/document/9303863/.

[3] B. Amos and J. Z. Kolter. OptNet: Differentiable Optimization as a Layer in Neural Networks. In *Proceedings of the 34th International Conference on Machine Learning*, pages 136–145. PMLR, July 2017. URL https://proceedings.mlr.press/v70/amos17a.html. ISSN: 2640-3498.

[4] B. Amos, L. Xu, and J. Z. Kolter. Input Convex Neural Networks, June 2017. URL http://arxiv.org/abs/1609.07152. arXiv:1609.07152 [cs, math].

[5] A. N. Angelopoulos and S. Bates. Conformal Prediction: A Gentle Introduction. *Foundations and Trends® in Machine Learning*, 16(4):494–591, 2023. ISSN 1935-8237. doi: 10.1561/2200000101. URL http://dx.doi.org/10.1561/2200000101.

[6] A. Ben-Tal, L. E. Ghaoui, and A. Nemirovski. *Robust Optimization*. Princeton University Press, 2009. ISBN 978-0-691-14368-2. URL https://www.jstor.org/stable/j.ctt7sk8p.

[7] D. Bertsimas and A. Thiele. Robust and Data-Driven Optimization: Modern Decision Making Under Uncertainty. In *Models, Methods, and Applications for Innovative Decision Making*, INFORMS TutORials in Operations Research, pages 95–122. INFORMS, Sept. 2006. ISBN 978-1-877640-20-9. doi: 10.1287/educ.1063.0022. URL https://pubsonline.informs.org/doi/abs/10.1287/educ.1063.0022. Section: 4.

[8] D. Bertsimas, E. Litvinov, X. A. Sun, J. Zhao, and T. Zheng. Adaptive Robust Optimization for the Security Constrained Unit Commitment Problem. *IEEE Transactions on Power Systems*, 28(1):52–63, Feb. 2013. ISSN 1558-0679. doi: 10.1109/TPWRS.2012.2205021. URL https://ieeexplore.ieee.org/document/6248193. Conference Name: IEEE Transactions on Power Systems.

[9] D. Bertsimas, V. Gupta, and N. Kallus. Data-driven robust optimization. *Mathematical Programming*, 167(2):235–292, Feb. 2018. ISSN 1436-4646. doi: 10.1007/s10107-017-1125-8. URL https://doi.org/10.1007/s10107-017-1125-8.

[10] C. Blundell, J. Cornebise, K. Kavukcuoglu, and D. Wierstra. Weight Uncertainty in Neural Networks. In *Proceedings of the 32nd International Conference on Machine Learning*, volume 37 of *Proceedings of Machine Learning Research*, pages 1613–1622. PMLR, May 2015. URL http://arxiv.org/abs/1505.05424. arXiv:1505.05424 [cs, stat] type: article.

[11] Y. Chen, Y. Shi, and B. Zhang. Optimal Control Via Neural Networks: A Convex Approach. In *International Conference on Learning Representations*, 2019. URL https://openreview.net/forum?id=H1MW72AcK7.

[12] A. Chenreddy and E. Delage. End-to-end Conditional Robust Optimization. Mar. 2024. doi: 10.48550/arXiv.2403.04670. URL https://openreview.net/forum?id=Oe9ngGi8Gh. arXiv:2403.04670 [cs].

[13] A. R. Chenreddy, N. Bandi, and E. Delage. Data-Driven Conditional Robust Optimization. In *Advances in Neural Information Processing Systems*, volume 35, pages 9525–9537, Dec. 2022. URL https://proceedings.neurips.cc/paper_files/paper/2022/hash/3df874367ce2c43891aab1ab23ae6959-Abstract-Conference.html.

[14] N. Christianson, L. Werner, A. Wierman, and S. Low. Dispatch-aware planning for feasible power system operation. *Electric Power Systems Research*, 212:108597, Nov. 2022. ISSN 0378-7796. doi: 10.1016/j.epsr.2022.108597. URL https://www.sciencedirect.com/science/article/pii/S0378779622006733.

[15] P. L. Donti, B. Amos, and J. Z. Kolter. Task-based End-to-end Model Learning in Stochastic Optimization. In *Advances in Neural Information Processing Systems*, volume 30, Long Beach, CA, USA, Dec. 2017. Curran Associates, Inc. doi: 10.48550/arXiv.1703.04529. URL http://arxiv.org/abs/1703.04529. arXiv:1703.04529 [cs].

[16] Y. Dvorkin. A Chance-Constrained Stochastic Electricity Market. *IEEE Transactions on Power Systems*, 35(4):2993–3003, July 2020. ISSN 1558-0679. doi: 10.1109/TPWRS.2019.2961231. URL https://ieeexplore.ieee.org/document/8937824. Conference Name: IEEE Transactions on Power Systems.

[17] B.-S. Einbinder, Y. Romano, M. Sesia, and Y. Zhou. Training Uncertainty-Aware Classifiers with Conformalized Deep Learning. In *Advances in Neural Information Processing Systems*, New Orleans, LA, USA, Nov. 2022. doi: 10.48550/arXiv.2205.05878. URL http://arxiv.org/abs/2205.05878. arXiv:2205.05878 [cs, stat].

[18] A. N. Elmachtoub, H. Lam, H. Zhang, and Y. Zhao. Estimate-Then-Optimize versus Integrated-Estimation-Optimization versus Sample Average Approximation: A Stochastic Dominance Perspective, Aug. 2023. URL http://arxiv.org/abs/2304.06833. arXiv:2304.06833 [cs, stat].

[19] Y. Gal and Z. Ghahramani. Dropout as a Bayesian Approximation: Representing Model Uncertainty in Deep Learning. In *arXiv:1506.02142 [cs, stat]*, Oct. 2016. URL http://arxiv.org/abs/1506.02142. arXiv: 1506.02142.

[20] M. Goerigk and J. Kurtz. Data-driven robust optimization using deep neural networks. *Computers & Operations Research*, 151:106087, Mar. 2023. ISSN 0305-0548. doi: 10.1016/j.cor.2022.106087. URL https://www.sciencedirect.com/science/article/pii/S0305054822003173.

[21] C. Gregory, K. Darby-Dowman, and G. Mitra. Robust optimization and portfolio selection: The cost of robustness. *European Journal of Operational Research*, 212(2):417–428, July 2011. ISSN 0377-2217. doi: 10.1016/j.ejor.2011.02.015. URL https://www.sciencedirect.com/science/article/pii/S0377221711001469.

[22] C. Johnstone and B. Cox. Conformal uncertainty sets for robust optimization. In *Proceedings of the Tenth Symposium on Conformal and Probabilistic Prediction and Applications*, pages 72–90. PMLR, Sept. 2021. URL https://proceedings.mlr.press/v152/johnstone21a.html. ISSN: 2640-3498.

[23] D. P. Kingma and J. Ba. Adam: A Method for Stochastic Optimization. In *International Conference on Learning Representations*, San Diego, CA, USA, May 2015. URL http://arxiv.org/abs/1412.6980.

[24] V. Kuleshov, N. Fenner, and S. Ermon. Accurate Uncertainties for Deep Learning Using Calibrated Regression. In *Proceedings of the 35th International Conference on Machine Learning*, pages 2796–2804. PMLR, July 2018. URL https://proceedings.mlr.press/v80/kuleshov18a.html. ISSN: 2640-3498.

[25] B. Lakshminarayanan, A. Pritzel, and C. Blundell. Simple and Scalable Predictive Uncertainty Estimation using Deep Ensembles. In *Advances in Neural Information Processing Systems*, volume 30. Curran Associates, Inc., 2017. URL https://proceedings.neurips.cc/paper/2017/hash/9ef2ed4b7fd2c810847ffa5fa85bce38-Abstract.html.

[26] A. Lin and D. E. Ba. How to Train Your FALCON: Learning Log-Concave Densities with Energy-Based Neural Networks. July 2023. URL https://openreview.net/forum?id=UP1r5-t-ov.

[27] J. Liu, Z. Lin, S. Padhy, D. Tran, T. Bedrax Weiss, and B. Lakshminarayanan. Simple and Principled Uncertainty Estimation with Deterministic Deep Learning via Distance Awareness. volume 33, pages 7498–7512. Curran Associates, Inc., 2020. URL https://proceedings.neurips.cc/paper/2020/hash/543e83748234f7cbab21aa0ade66565f-Abstract.html.

[28] Z. Nado, N. Band, M. Collier, J. Djolonga, M. W. Dusenberry, S. Farquhar, Q. Feng, A. Filos, M. Havasi, R. Jenatton, G. Jerfel, J. Liu, Z. Mariet, J. Nixon, S. Padhy, J. Ren, T. G. J. Rudner, F. Sbahi, Y. Wen, F. Wenzel, K. Murphy, D. Sculley, B. Lakshminarayanan, J. Snoek, Y. Gal, and D. Tran. Uncertainty Baselines: Benchmarks for Uncertainty & Robustness in Deep Learning. Jan. 2022. doi: 10.48550/arXiv.2106.04015. URL http://arxiv.org/abs/2106.04015. arXiv:2106.04015 [cs].

[29] M. Ndrio, A. N. Madavan, and S. Bose. Pricing Conditional Value at Risk-Sensitive Economic Dispatch. In *2021 IEEE Power & Energy Society General Meeting (PESGM)*, pages 01–05, July 2021. doi: 10.1109/PESGM46819.2021.9637845. URL https://ieeexplore.ieee.org/document/9637845. ISSN: 1944-9933.

[30] A. Nemirovski and A. Shapiro. Convex Approximations of Chance Constrained Programs. *SIAM Journal on Optimization*, 17(4):969–996, Jan. 2007. ISSN 1052-6234, 1095-7189. doi: 10.1137/050622328. URL http://epubs.siam.org/doi/10.1137/050622328.

[31] S. S. Parvar and H. Nazaripouya. Optimal Operation of Battery Energy Storage Under Uncertainty Using Data-Driven Distributionally Robust Optimization. *Electric Power Systems Research*, 211:108180, Oct. 2022. ISSN 0378-7796. doi: 10.1016/j.epsr.2022.108180. URL https://www.sciencedirect.com/science/article/pii/S0378779622003911.

[32] Y. P. Patel, S. Rayan, and A. Tewari. Conformal Contextual Robust Optimization. In *Proceedings of The 27th International Conference on Artificial Intelligence and Statistics*, pages 2485–2493. PMLR, Apr. 2024. URL https://proceedings.mlr.press/v238/p-patel24a.html. ISSN: 2640-3498.

[33] B. K. Poolla, A. R. Hota, S. Bolognani, D. S. Callaway, and A. Cherukuri. Wasserstein Distributionally Robust Look-Ahead Economic Dispatch. *IEEE Transactions on Power Systems*, 36(3):2010–2022, May 2021. ISSN 1558-0679. doi: 10.1109/TPWRS.2020.3034488. URL https://ieeexplore.ieee.org/document/9242289. Conference Name: IEEE Transactions on Power Systems.

[34] A. G. Quaranta and A. Zaffaroni. Robust optimization of conditional value at risk and portfolio selection. *Journal of Banking & Finance*, 32(10):2046–2056, Oct. 2008. ISSN 0378-4266. doi: 10.1016/j.jbankfin.2007.12.025. URL https://www.sciencedirect.com/science/article/pii/S0378426607004281.

[35] H. Rahimian and S. Mehrotra. Distributionally Robust Optimization: A Review. *arXiv:1908.05659 [cs, math, stat]*, Aug. 2019. URL http://arxiv.org/abs/1908.05659. arXiv: 1908.05659.

[36] C. E. Rasmussen and C. K. I. Williams. *Gaussian Processes for Machine Learning*. The MIT Press, Nov. 2005. ISBN 978-0-262-25683-4. doi: 10.7551/mitpress/3206.001.0001. URL https://doi.org/10.7551/mitpress/3206.001.0001.

[37] Y. Romano, E. Patterson, and E. Candes. Conformalized Quantile Regression. In H. Wallach, H. Larochelle, A. Beygelzimer, F. d. Alché-Buc, E. Fox, and R. Garnett, editors, *Advances in Neural Information Processing Systems*, volume 32. Curran Associates, Inc., 2019. URL http://papers.neurips.cc/paper/8613-conformalized-quantile-regression.pdf.

[38] G. Shafer and V. Vovk. A Tutorial on Conformal Prediction. *Journal of Machine Learning Research*, 9(12): 371–421, 2008. URL http://jmlr.org/papers/v9/shafer08a.html.

[39] A. Shapiro, D. Dentcheva, and A. Ruszczyński. *Lectures on Stochastic Programming: Modeling and Theory*. Society for Industrial and Applied Mathematics, Jan. 2009. ISBN 978-0-89871-687-0 978-0-89871-875-1. doi: 10.1137/1.9780898718751. URL http://epubs.siam.org/doi/book/10.1137/1.9780898718751.

[40] D. Stutz, Krishnamurthy, Dvijotham, A. T. Cemgil, and A. Doucet. Learning Optimal Conformal Classifiers, May 2022. URL http://arxiv.org/abs/2110.09192. arXiv:2110.09192 [cs, stat].

[41] C. Sun, L. Liu, and X. Li. Predict-then-Calibrate: A New Perspective of Robust Contextual LP. Nov. 2023. URL https://openreview.net/forum?id=TnTDiCppx5&referrer=%5Bthe%20profile%20of%20Chunlin%20Sun%5D(%2Fprofile%3Fid%3D~Chunlin_Sun1).

[42] I. Wang, C. Becker, B. Van Parys, and B. Stellato. Learning Decision-Focused Uncertainty Sets in Robust Optimization, Apr. 2024. URL http://arxiv.org/abs/2305.19225. arXiv:2305.19225 [math].

[43] J. Warrington, P. J. Goulart, S. Mariéthoz, and M. Morari. Robust reserve operation in power systems using affine policies. In *2012 IEEE 51st IEEE Conference on Decision and Control (CDC)*, pages 1111–1117, Dec. 2012. doi: 10.1109/CDC.2012.6425913. URL https://ieeexplore.ieee.org/abstract/document/6425913. ISSN: 0743-1546.

[44] A. G. Wilson, Z. Hu, R. Salakhutdinov, and E. P. Xing. Deep Kernel Learning. In A. Gretton and C. C. Robert, editors, *Proceedings of the 19th International Conference on Artificial Intelligence and Statistics (AISTATS)*, pages 370–378, Cadiz, Spain, May 2016. PMLR. URL http://proceedings.mlr.press/v51/wilson16.html. ISSN: 1938-7228.

[45] X. Yan, C. Gu, X. Zhang, and F. Li. Robust Optimization-Based Energy Storage Operation for System Congestion Management. *IEEE Systems Journal*, 14(2):2694–2702, June 2020. ISSN 1932-8184, 1937-9234, 2373-7816. doi: 10.1109/JSYST.2019.2932897. URL https://ieeexplore.ieee.org/document/8805255/.

[46] Q. P. Zheng, J. Wang, and A. L. Liu. Stochastic Optimization for Unit Commitment—A Review. *IEEE Transactions on Power Systems*, 30(4):1913–1924, July 2015. ISSN 1558-0679. doi: 10.1109/TPWRS.2014.2355204. URL https://ieeexplore.ieee.org/document/6912028. Conference Name: IEEE Transactions on Power Systems.

[47] W. Zhong, K. Xie, Y. Liu, S. Xie, and L. Xie. Chance Constrained Scheduling and Pricing for Multi-Service Battery Energy Storage. *IEEE Transactions on Smart Grid*, 12(6):5030–5042, Nov. 2021. ISSN 1949-3061. doi: 10.1109/TSG.2021.3109140. URL https://ieeexplore.ieee.org/document/9525453. Conference Name: IEEE Transactions on Smart Grid.

A   Appendix: Related Work

Task-based learning.   The notion of "task-based" end-to-end model learning was introduced by Donti et al. [15], which proposed to train machine learning models end-to-end in a manner capturing a downstream stochastic optimization task. To achieve this, the authors backpropagate gradients through a stochastic optimization problem, which is made possible for various types of convex optimization problems via the implicit function theory [15, 3, 1]. However, Donti et al. [15] does not train the model to estimate uncertainty and thereby does not provide any explicit guarantees on robustness on their decisions to uncertainty. Our framework improves upon this baseline by yielding calibrated uncertainty sets which can then be used to obtain robust decisions.

Uncertainty Quantification.   Various designs for deep learning regression models that provide uncertainty estimates have been proposed in the literature, including Bayesian neural networks [10, 19], Gaussian process regression and deep kernel learning [36, 44, 27], ensembles of models [25], and quantile regression [37], among other techniques. These methods typically only provide heuristic uncertainty estimates that are not necessarily well-calibrated [28].

Post-hoc methods such as isotonic regression [24] or conformal prediction [38] may be used to calibrate the uncertainty outputs of deep learning models. These calibration methods generally treat the model as a black box and scale predicted uncertainty levels so that they are calibrated on a held-out calibration set. Isotonic regression guarantees calibrated outputs in the limit of infinite data, whereas conformal methods provide probabilistic, finite-sample calibration guarantees when the calibration set is exchangeable with (*e.g.*, drawn i.i.d. from the same distribution as) the test data. These calibration methods are generally not included in the model training procedure because they involve non-differentiable operators, such as sorting. However, recent works have proposed differentiable losses [17, 40] that approximate the conformal prediction procedure during training and thus allow end-to-end training of models to output more calibrated uncertainty. As approximations, these methods lose the marginal coverage guarantees that true conformal methods provide. However, such guarantees can be recovered at test time by replacing the approximations with true conformal prediction.

Robust and stochastic optimization.   The optimization community has proposed a number of techniques over the years to improve robust decision-making under uncertainty, including stochastic, risk-sensitive, chance-constrained, distributionally robust, and robust optimization (*e.g.*, [6, 39, 30, 35]). These techniques have been applied to a wide range of applications, including energy systems operation [46, 29, 16, 47, 33, 43, 8, 14] and portfolio optimization [21, 34, 9]. In these works, the robust and stochastic optimization methods enable selecting decisions (grid resource dispatches or portfolio allocations) in a manner that is aware of uncertainty, *e.g.*, so an energy system operator can ensure that sufficient generation is available to meet demand even on a cloudy day without much solar generation. Typically, however, the construction of uncertainty sets, estimated probability distributions over uncertain parameters, or ambiguity sets over distributions takes place offline and is unconnected to the eventual decision-making task. Thus, our proposed end-to-end approach allows for simultaneous calibration of uncertainty sets with optimal decision-making.

B   Appendix: Maximizing over the uncertainty set

We consider robust optimization problems of the form

$$\min_{z\in\mathbb{R}^p} \max_{\hat{y}\in\mathbb{R}^n} \hat{y}^\top F z + \tilde{f}(x,z) \qquad \text{s.t.} \qquad \hat{y}\in\Omega(x), \quad g(x,z)\leq 0.$$

For fixed z, the inner maximization problem is

$$\max_{\hat{y}\in\mathbb{R}^n} \hat{y}^\top F z \qquad \text{s.t.} \qquad \hat{y}\in\Omega(x),$$

which we analyze in the more abstract form

$$\max_{y\in\mathbb{R}^n} c^\top y \qquad \text{s.t.} \qquad y\in\Omega$$

for arbitrary $c \in \mathbb{R}^n \setminus \{0\}$. The subsections of this appendix derive the dual form of this maximization problem for specific representations of the uncertainty set Ω.

Suppose y is standardized or whitened by an affine transformation with $\mu \in \mathbb{R}^n$ and invertible matrix $W \in \mathbb{R}^{n \times n}$

$$y_{\text{transformed}} = W^{-1}(y - \mu)$$

so that Ω is an uncertainty set on the transformed $y_{\text{transformed}}$. Then, the original primal objective can be recovered as

$$c^\top y = c^\top (W y_{\text{transformed}} + \mu) = (Wc)^\top y_{\text{transformed}} + c^\top \mu.$$

In our experiments, we use element-wise standardization of y by setting $W = \text{diag}(y_{\text{std}})$, where $y_{\text{std}} \in \mathbb{R}^n$ is the element-wise standard-deviation of y.

B.1 Maximizing over a box constraint

Let $[\underline{y}, \bar{y}] \subset \mathbb{R}^n$ be a box uncertainty set for $y \in \mathbb{R}^n$. Then, for any vector $c \in \mathbb{R}^n$, the primal linear program

$$\max_{y \in \mathbb{R}^n} c^\top y \qquad \text{s.t.} \qquad \underline{y} \le y \le \bar{y}$$

has dual problem

$$\min_{v \in \mathbb{R}^{2n}} \begin{bmatrix} \bar{y}^\top & -\underline{y}^\top \end{bmatrix} v \qquad \text{s.t.} \qquad \begin{bmatrix} I_n & -I_n \end{bmatrix} v = c, \quad v \ge \mathbf{0},$$

which can also be equivalently written as

$$\min_{v \in \mathbb{R}^n} (\bar{y} - \underline{y})^\top v + \underline{y}^\top c \qquad \text{s.t.} \qquad v \ge \mathbf{0}, \quad v - c \ge \mathbf{0}.$$

Since strong duality always holds for linear programs, the optimal values of the primal and dual problems will be equal so long as one of the problems is feasible, *e.g.*, so long as the box $[\underline{y}, \bar{y}]$ is nonempty. We can thus incorporate this dual problem into the outer minimization of (1) to yield the non-robust form (4).

B.2 Maximizing over an ellipsoid

For any $c \in \mathbb{R}^n \setminus \{0\}$, $\Sigma \in \mathbb{S}^n_{++}$, and $q > 0$, the primal quadratically constrained linear program (QCLP)

$$\max_{y \in \mathbb{R}^n} c^\top y \qquad \text{s.t.} \qquad (y - \mu)^\top \Sigma^{-1}(y - \mu) \le q$$

has dual problem

$$\min_{v \in \mathbb{R}} \frac{1}{4v} c^\top \Sigma c + \mu^\top c + vq \qquad \text{s.t.} \quad v > 0.$$

By Slater's condition, strong duality holds by virtue of the assumption that $q > 0$ (which implies strict feasibility of the primal problem), and thus the primal and dual problems have the same optimal value. Moreover, since Σ is positive definite and $q > 0$, this problem has a unique optimal solution at $v^\star = \frac{1}{2\sqrt{q}} \|\Sigma^{1/2} c\|_2$. Substituting $v^\star$ into the dual problem objective yields a dual optimal value of

$$\sqrt{q} \|\Sigma^{1/2} c\|_2 + \mu^\top c,$$

and incorporating this optimal value into the outer minimization of (1) yields the non-robust form (5).

B.3 Proof of Theorem 1: Maximizing over the sublevel set of a PICNN

Let $s_\theta : \mathbb{R}^m \times \mathbb{R}^n \to \mathbb{R}$ be a partially input-convex neural network (PICNN) with ReLU activations as described in (6), so that $s_\theta(x, y)$ is convex in y. Suppose that all the hidden layers have the same dimension d (*i.e.*, $\forall l = 0, \ldots, L-1$: $W_l \in \mathbb{R}^{d \times d}$, $V_l \in \mathbb{R}^{d \times n}$, $b_l \in \mathbb{R}^d$), and the final layer L has $W_L \in \mathbb{R}^{1 \times d}$, $V_L \in \mathbb{R}^{1 \times n}$, $b_L \in \mathbb{R}$. Let $c \in \mathbb{R}^n$ be any vector.

Then, the optimization problem

$$\max_{y \in \mathbb{R}^n} c^\top y \qquad \text{s.t.} \qquad s_\theta(x, y) \leq q \tag{8}$$

can be equivalently written as

$$\max_{y \in \mathbb{R}^n, \ \sigma_1, \dots, \sigma_L \in \mathbb{R}^d} c^\top y \tag{9a}$$

$$\text{s.t.} \quad \sigma_l \geq \mathbf{0}_d \qquad\qquad\qquad \forall l = 1, \dots, L \tag{9b}$$

$$\sigma_{l+1} \geq W_l \sigma_l + V_l y + b_l \qquad\qquad \forall l = 0, \dots, L-1 \tag{9c}$$

$$W_L \sigma_L + V_L y + b_L \leq q, \tag{9d}$$

To see that this is the case, first note that (9) is a relaxed form of (8), obtained by replacing the equalities $\sigma_{l+1} = \text{ReLU}(W_l \sigma_l + V_l y + b_l)$ in the definition of the PICNN (6) with the two separate inequalities $\sigma_{l+1} \geq \mathbf{0}_d$ and $\sigma_{l+1} \geq W_l \sigma_l + V_l y + b_l$ for each $l = 0, \dots, L-1$. As such, the optimal value of (9) is no less than that of (8). However, given an optimal solution $y, \sigma_1, \dots, \sigma_L$ to (9), it is possible to obtain another feasible solution $y, \hat{\sigma}_1, \dots, \hat{\sigma}_L$ with the same optimal objective value by iteratively decreasing each component of σ_l until one of the two inequality constraints (9b), (9c) is tight, beginning at $l = 1$ and incrementing l once all entries of σ_l cannot be decreased further. This procedure of decreasing the entries in each σ_l will maintain problem feasibility, since the weight matrices W_l are all assumed to be entrywise nonnegative in the PICNN construction; in particular, this procedure will not increase the left-hand side of (9d). Moreover, since one of the two constraints (9b), (9c) will hold for each entry of each $\hat{\sigma}_l$, this immediately implies that y is feasible for the unrelaxed problem (8), and so (8) and (9) must have the same optimal value.

Having shown that we may replace the convex program (8) with a linear equivalent (9), we can write this latter problem in the matrix form

$$\max_{y \in \mathbb{R}^n, \ \sigma_1, \dots, \sigma_L \in \mathbb{R}^d} c^\top y \qquad \text{s.t.} \qquad A \begin{bmatrix} y \\ \sigma_1 \\ \vdots \\ \sigma_L \end{bmatrix} \leq b$$

where

$$A = \begin{bmatrix} & -I_d & & & \\ & & \ddots & & \\ & & & -I_d & \\ V_0 & -I_d & & & \\ \vdots & W_1 & \ddots & & \\ \vdots & & \ddots & -I_d \\ V_L & & & W_L \end{bmatrix} \in \mathbb{R}^{(2Ld+1) \times (n+Ld)}, \qquad b = \begin{bmatrix} \mathbf{0}_d \\ \vdots \\ \mathbf{0}_d \\ -b_0 \\ \vdots \\ -b_{L-1} \\ q - b_L \end{bmatrix} \in \mathbb{R}^{2Ld+1}. \tag{10}$$

By strong duality, if this linear program has an optimal solution, its optimal value is equal to the optimal value of its dual problem:

$$\min_{v \in \mathbb{R}^{2Ld+1}} b^\top v \qquad \text{s.t.} \qquad A^\top v = \begin{bmatrix} c \\ \mathbf{0}_{Ld} \end{bmatrix}, \quad v \geq 0. \tag{11}$$

We can incorporate this dual problem (11) into the outer minimization of (1) to yield the non-robust form (7). For a more interpretable form of this dual problem, let $v^{(i)}$ denote the portion of the dual vector v corresponding to the i-th block-row of matrix A, indexed from 0. That is, $v^{(i)} = v_{id+1:(i+1)d}$ for $i = 0, \dots, 2L-1$. Furthermore, let $\mu = v_{2Ld+1}$

be the last entry of v. Written out, the dual problem (11) becomes

$$\min_{v^{(0)},\ldots,v^{(2L-1)}\in\mathbb{R}^d,\mu\in\mathbb{R}} \quad \mu(q-b_L) - \sum_{l=0}^{L} b_l^\top v^{(L+l)}$$

$$\text{s.t.} \quad \begin{bmatrix} V_0^\top & \cdots & V_L^\top \end{bmatrix} v_{Ld+1:} = c$$

$$W_{l+1}^\top v^{(L+l+1)} - v^{(L+l)} - v^{(l)} = \mathbf{0}_d \qquad \forall l = 0,\ldots,L-1$$

$$v \geq 0.$$

B.4 Ensuring feasibility of the PICNN maximization problem

As noted at the end of Section 3.2, it may sometimes be the case that the inner maximization problem of (1) is unbounded or infeasible when $\Omega_\theta(x)$ is parametrized by a PICNN, since in general, the sublevel sets of the PICNN might be unbounded, or the q selected by the split conformal procedure detailed in Section 3.1 may be sufficiently small that $\Omega_\theta(x) = \{\hat{y} \in \mathbb{R}^n \mid s_\theta(x,\hat{y}) \leq q\}$ is empty for certain inputs x. We can address each of these concerns using separate techniques.

Ensuring compact sublevel sets   To ensure that the PICNN-parametrized score function $s_\theta(x,y)$ has compact sublevel sets in y, we can redefine the output layer by setting $V_L = \mathbf{0}_{1 \times n}$ and adding a small ℓ^∞ norm term penalizing growth in y:

$$s_\theta(x,y) = W_L \sigma_L + \varepsilon \|y\|_\infty + b_L, \tag{12}$$

where $\varepsilon \geq 0$ is a small penalty term, and where all the remaining parameters and layers remain identical to their definition in (6). This modification ensures that, for any fixed x, $s_\theta(x,y)$ has compact sublevel sets, since $\sigma_L \geq 0$ by construction (6) and the penalty term $\varepsilon\|y\|_\infty$ will grow unboundedly large as y goes to infinity in any direction, so long as $\varepsilon > 0$. Moreover, so long as ε is chosen sufficiently small and the PICNN is sufficiently deep, this modification should not negatively impact the ability of the PICNN to represent general compact convex uncertainty sets.

Using this modified PICNN (12), the maximization problem (8) can be written as an equivalent linear program

$$\max_{\substack{y\in\mathbb{R}^n,\ \sigma_1,\ldots,\sigma_L\in\mathbb{R}^d, \\ \kappa\in\mathbb{R}}} \quad c^\top y \tag{13a}$$

$$\text{s.t.} \quad \sigma_l \geq \mathbf{0}_d \qquad\qquad\qquad \forall l = 1,\ldots,L \tag{13b}$$

$$\sigma_{l+1} \geq W_l \sigma_l + V_l y + b_l \qquad \forall l = 0,\ldots,L-1 \tag{13c}$$

$$\kappa \geq y_i,\ \kappa \geq -y_i \qquad\qquad \forall i = 1,\ldots,n \tag{13d}$$

$$W_L \sigma_L + \varepsilon\kappa + b_L \leq q \tag{13e}$$

where the equivalence between (8) and (13) follows the same argument as that employed in the previous section when showing the equivalence of (8) and (9). We can thus likewise apply strong duality to obtain an equivalent minimization form of the problem (13) and incorporate this into the outer minimization of (1) to yield a non-robust problem of the general form (7).

Ensuring $\Omega_\theta(x)$ is nonempty   If the q chosen by the split conformal procedure is too small such that $\Omega_\theta(x)$ is empty, i.e., $q \leq q_{\min}$ where

$$q_{\min} := \min_{\hat{y}\in\mathbb{R}^n} s_\theta(x,\hat{y}), \tag{14}$$

then we simply increase q to $q_{\min}$ so that $\Omega_\theta(x)$ is guaranteed to be nonempty. That is, for input x, we set

$$q = \max\left(\min_{\hat{y}\in\mathbb{R}^n} s_\theta(x,\hat{y}),\ \text{QUANTILE}\left(\{s_\theta(x_i,y_i)\}_{(x_i,y_i)\in D_{\text{cal}}},\ 1-\alpha\right) \right).$$

This preserves the marginal coverage guarantee, as increasing q can only result in a larger uncertainty set $\Omega_\theta(x)$.

In theory, $q_{\min}$ varies as a function of θ, and it is possible to differentiate through the optimization problem (14) using the methods from Agrawal et al. [1] since the problem is convex and s_θ is assumed to be differentiable w.r.t. θ almost everywhere. However, to avoid this added complexity, in practice, we treat $q_{\min}$ as a constant. In other words, on inputs x where we have to increase q to $q_{\min}$, we treat $\frac{\partial q}{\partial \theta} = 0$.

C Appendix: Exact differentiable conformal prediction

In this section, we prove how to exactly differentiate through the conformal prediction procedure, unlike the approximate derivative first introduced in [40].

Theorem 2. Let $\alpha \in (0,1)$ be a risk level, and let $s_i := s_\theta(x_i, y_i)$ denote the scores computed by a score function $s_\theta : \mathbb{R}^m \times \mathbb{R}^n \to \mathbb{R}$ over data points $\{(x_i, y_i)\}_{i=1}^M$. Suppose $s_\theta(x_i, y_i)$ is differentiable w.r.t. θ for all $i = 1, \ldots, M$.

Define $s_{M+1} := \infty$. Let $\sigma : \{1, \ldots, M+1\} \to \{1, \ldots, M+1\}$ denote the permutation that sorts the scores in ascending order, such that $s_{\sigma(i)} \leq s_{\sigma(j)}$ for all $i < j$. For simplicity of notation, we may write $s_{(i)} := s_{\sigma(i)}$.

Let $q = \text{QUANTILE}(\{s_i\}_{i=1}^M, 1-\alpha)$ where the QUANTILE function is as defined in Algorithm 1. That is, $q = s_{(k)}$, where $k := \lceil (M+1)(1-\alpha) \rceil \in \{1, \ldots, M, M+1\}$. If $s_{(k)}$ is unique, then

$$\frac{dq}{d\theta} = \begin{cases} \frac{d}{d\theta} s_\theta(x_{\sigma(k)}, y_{\sigma(k)}), & \text{if } \alpha \geq \frac{1}{M+1} \\ 0, & \text{otherwise.} \end{cases}$$

Proof. First, when $\alpha \in (0, \frac{1}{M+1})$, we have $k = M+1$, so $q = \infty$ is constant regardless of the choice of θ. Thus, $\frac{dq}{d\theta} = 0$.

Now, suppose $\alpha \geq \frac{1}{M+1}$. The QUANTILE function returns the k-th largest value of $\{s_i\}_{i=1}^M \cup \{\infty\}$. Since we assume $s_{(k)}$ is unique, we have $\frac{dq}{ds_{(i)}} = \mathbf{1}[i = k]$. Finally, we have

$$\frac{dq}{d\theta} = \sum_{i=1}^M \frac{dq}{ds_i} \frac{ds_i}{d\theta} = \sum_{i=1}^M \frac{dq}{ds_{(i)}} \frac{ds_{(i)}}{d\theta} = \frac{ds_{(k)}}{d\theta} = \frac{d}{d\theta} s_\theta(x_{\sigma(k)}, y_{\sigma(k)}).$$

$\square$

The two key assumptions in this theorem are that (1) s_θ is differentiable w.r.t. θ, and (2) $s_{(k)}$ is unique. When s_θ is a neural network with a common activation function (*e.g.*, ReLU), (1) holds for inputs $(x, y) \in \mathbb{R}^m \times \mathbb{R}^n$ almost everywhere and θ almost everywhere. Regarding (2), in practice, just as the gradient of the max function is typically implemented without checking whether its inputs have ties, we do not check whether $s_{(k)}$ is unique.

D Appendix: Experiment details

Our experiments were conducted across a variety of machines, including private servers and Amazon AWS EC2 instances, ranging from 12-core to 128-core machines. Our ETO experiments benefited from GPU acceleration across a combination of NVIDIA GeForce GTX 1080 Ti, Titan RTX, T4, and A100 GPUs. Our E2E experiments did not use GPU acceleration, due to the lack of GPU support in the `cvxpylayers` [1] Python package.

In all experiments, we use a batch size of 256 and the Adam [23] optimizer.

For all `ETO` baseline models, we performed a hyperparameter grid search over learning rates ($10^{-4.5}$, 10^{-4}, $10^{-3.5}$, 10^{-3}, $10^{-2.5}$, 10^{-2}, $10^{-1.5}$) and L2 weight decay values (0, 10^{-4}, 10^{-3}, 10^{-2}). Models were trained for up to 100 epochs with early stopping if there was no improvement in validation loss for 10 consecutive epochs.

D.1 Uncertainty representation

Box uncertainty Our box uncertainty model uses a neural network h_θ with 3 hidden layers of 256 units each and ReLU activations with batch-normalization. The output layer has dimension $2n$, where dimensions $1:n$ predict the

lower bound. Output dimensions $n+1:2n$, after passing through a softplus to ensure positivity, represents the difference between the upper and lower bounds. That is,

$$\begin{bmatrix} h_\theta^{\mathrm{lo}}(x) \\ h_\theta^{\mathrm{hi}}(x) \end{bmatrix} = \begin{bmatrix} h_\theta(x)_{1:n} \\ h_\theta(x)_{1:n} + \mathrm{softplus}(h_\theta(x)_{n+1:2n}) \end{bmatrix}.$$

This architecture ensures that $h_\theta^{\mathrm{hi}}(x) > h_\theta^{\mathrm{lo}}(x)$.

In the two-stage ETO baseline, we first train h_θ to estimate the $\alpha/2$- and $(1-\alpha/2)$-quantiles, so that $[h_\theta^{\mathrm{lo}}(x), h_\theta^{\mathrm{hi}}(x)]$ represents the centered $(1-\alpha)$-confidence region. Quantile regression [37] is a common method for generating uncertainty sets for scalar predictions by estimating quantiles of the conditional distribution $\mathscr{P}(y \mid x)$. For scalar true label y, quantile regression models are commonly trained to minimize *pinball loss* (a.k.a. *quantile loss*) where β is the quantile level being estimated:

$$\mathrm{pinball}_\beta(\hat{y}, y) = \begin{cases} \beta \cdot (y - \hat{y}), & \text{if } y > \hat{y} \\ (1-\beta) \cdot (\hat{y} - y), & \text{if } y \le \hat{y}, \end{cases}$$

To generalize the pinball loss to our setting of multi-dimensional $y \in \mathbb{R}^n$, we sum the pinball loss across the dimensions of y: $\mathrm{pinball}_\beta(\hat{y}, y) = \sum_{i=1}^n \mathrm{pinball}_\beta(\hat{y}_i, y_i)$.

Our end-to-end (E2E) box uncertainty models use the same architecture as above, initialized with weights from the the trained ETO model. We found it helpful to use a weighted combination of the task loss and pinball loss during training of the E2E models to improve training stability. In our experiments, we used a weight of 0.9 on the task loss and 0.1 on the pinball loss. The E2E models used the best L2 weight decay from the ETO models, and the learning rate was tuned across 10^{-2}, 10^{-3}, and 10^{-4}.

Ellipsoidal uncertainty   Our ellipsoidal uncertainty model uses a neural network h_θ with 3 hidden layers of 256 units each and ReLU activations with batch-normalization. The output layer has dimension $n + n(n+1)/2$, where dimensions $1:n$ predict the mean $\mu_\theta(x)$ and the remaining output dimensions are used to construct a lower-triangular Cholesky factor $L_\theta(x)$ of the covariance matrix $\Sigma_\theta(x) = L_\theta(x)L_\theta(x)^\top$. We pass the diagonal entries of L through a softplus function to ensure strict positivity, which then ensures $\Sigma_\theta(x)$ is positive definite.

For the ETO baseline, we trained the model using the negative log-likelihood (NLL) loss

$$\mathrm{NLL}(h_\theta(x), y) = -\ln \mathscr{N}(y \mid \mu_\theta(x), \Sigma_\theta(x)),$$

where $\mathscr{N}(\cdot \mid \mu, \Sigma)$ denotes the density of a multivariate normal distribution with mean μ and covariance matrix Σ.

Our end-to-end (E2E) ellipsoidal uncertainty models use the same architecture as above, initialized with weights from the the trained ETO model. We found it helpful to use a weighted combination of the task loss and NLL loss during training of the E2E models to improve training stability. In our experiments, we used a weight of 0.9 on the task loss and 0.1 on the NLL loss. The E2E models used the best L2 weight decay from the ETO models, and the learning rate was tuned across 10^{-2}, 10^{-3}, and 10^{-4}.

PICNN uncertainty   Our PICNN has 2 hidden layers with ReLU activations.

For the battery storage problem, we used 64 units per hidden layer. We did not run into any feasibility issues for the PICNN maximization problem, so we did not restrict V_L as described in Appendix B.4, and we set $\varepsilon = 0$.

For the portfolio optimization problem, we used 128 units per hidden layer. We did run into feasibility issues for the PICNN maximization problem, which we resolved by setting $V_L = \mathbf{0}_{1 \times n}$ as described in Appendix B.4. This change alone was sufficient, and we set $\varepsilon = 0$.

For the ETO baseline, we follow the approach by [26] to give probabilistic interpretation to a PICNN model s_θ via the energy-based model $\hat{\mathscr{P}}(y \mid x) \propto \exp(-s_\theta(x, y))$. We train our ETO PICNN models with an approximation to the true NLL loss $\mathrm{NLL}(s_\theta(x, y)) = -\ln \hat{\mathscr{P}}(y \mid x)$ based on samples from Metropolis-Adjusted Langevin Algorithm (MALA), a Markov Chain Monte Carlo (MCMC) method. We refer readers to our code on GitHub for the specific hyperparameters and implementation details we used.

Note that under this energy-based model, adding a scalar constant c to the PICNN (*i.e.*, $s_\theta(x,y)+c$) does not change the probability distribution. That is, $\exp(-s_\theta(x,y)) \propto \exp(-s_\theta(x,y)+c)$. To regularize the PICNN model, which has a bias term in its output layer, we therefore introduce a regularization loss of $w_{\text{zero}} \cdot s_\theta(x,y)^2$ where w_{zero} is a regularization weight. This regularization loss encourages $s_\theta(x,y)$ to be close to 0, for all examples in the training set. In our experiments, we set $w_{\text{zero}} = 1$.

Our end-to-end (E2E) PICNN uncertainty models use the same architecture as above, initialized with weights from the the trained ETO model. Unlike for box and ellipsoidal uncertainty which used a weighted combination of task loss and NLL loss, our E2E PICNN uncertainty models are trained only with the task loss. Similar to the ETO PICNN model, we also regularize the E2E PICNN. Here, we add a regularization loss of $w_q \cdot q^2$, where w_q is a regularization weight and q is the conformal prediction threshold computed in each minibatch of E2E training. This regularization loss term aims to keep q near 0; without this regularization, we found that q tended to grow dramatically over training epochs with poor task loss. In our experiments, we set $w_q = 0.01$. The E2E models used the best L2 weight decay from the ETO models, and the learning rate was tuned across 10^{-3} and 10^{-4}.

D.2 Data

Price forecasting for battery storage   We use the same dataset as Donti et al. [15] in our price forecasting for battery storage problem. In this dataset, the target $y \in \mathbb{R}^{24}$ is the hourly PJM day-ahead system energy price for 2011-2016, for a total of 2189 days. Unlike Donti et al. [15], though, we do not exclude any days whose electricity prices are too high (>500\$/MWh). Whereas Donti et al. [15] treated these days as outliers, our conditional robust optimization problem is designed to output robust decisions. For predicting target for a given day, the inputs $x \in \mathbb{R}^{101}$ include the previous day's log-prices, the given day's hourly load forecast, the previous day's hourly temperature, the given day's hourly temperature, and several calendar-based features such as whether the given day is a weekend or a US holiday.

For the setting without distribution shift, we take a random 20% subset of the dataset as the test set; because the test set is selected randomly, it is considered exchangeable with the rest of the dataset. For the setting with distribution shift, we take the chronologically last 20% of the dataset as the test set; because load, electricity prices, and temperature all have distribution shifts over time, the test set is not exchangeable with the rest of the dataset. For each seed, we further use a 80/20 random split of the remaining data for training and calibration.

Portfolio optimization   For the portfolio optimization task, we used synthetically generated data. We sample $x \in \mathbb{R}^2, y \in \mathbb{R}^2$ from a mixture of three 4-D multivariate Gaussian distributions as used in [12]. Formally,

$$\begin{bmatrix} x \\ y \end{bmatrix} \sim p_a \mathcal{N}(\mu_a, \Sigma_1) + p_b \mathcal{N}(\mu_b, \Sigma_b) + p_c \mathcal{N}(\mu_c, \Sigma_c)$$

where $p_a + p_b + p_c = 1$. Specifically,

$$p_a = \phi, \qquad\qquad p_b = \frac{1}{\alpha_{\text{GMM}}+1}(1-\phi), \qquad p_c = \frac{\alpha_{\text{GMM}}}{\alpha_{\text{GMM}}+1}(1-\phi),$$

$$\Sigma_a = \begin{bmatrix} 1 & 0 & 0.37 & 0 \\ 0 & 1.5 & 0 & 0 \\ 0.37 & 0 & 2 & 0.73 \\ 0 & 0 & 0.73 & 3 \end{bmatrix}, \qquad \Sigma_b = \alpha_{\text{GMM}}\Sigma_a, \qquad\qquad \Sigma_c = \frac{1}{\alpha_{\text{GMM}}}\Sigma_a$$

for some $\phi \in [0,1]$ and $\alpha_{\text{GMM}} \in [0,1]$. In our experiments, we used $\phi = 0.7$ and $\alpha_{\text{GMM}} = 0.9$ (it was unclear to us what values of ϕ and α_{GMM} were chosen by Chenreddy and Delage [12] for their experiments). For each random seed, we generate 2000 samples and use a (train, calibration, test) split of (600, 400, 1000).

D.3 Experimental results: Portfolio optimization

Figures 6 and 7 mirror Figures 2 and 3, except that the results here are on the portfolio problem with synthetic data. We again find that our E2E approach generally improves upon the ETO baselines at all uncertainty levels α, with the exception of box uncertainty where all the methods achieve similar performance. Our PICNN-based uncertainty
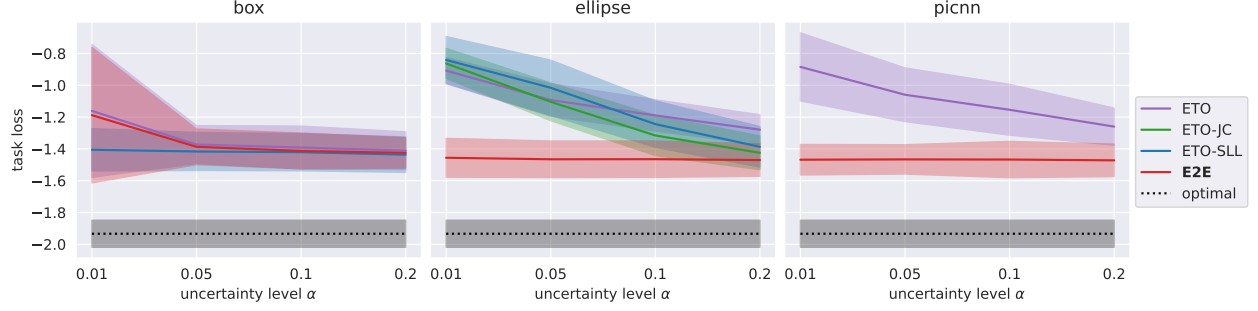
Figure 6: Task loss performance (mean ± 1 stddev across 10 runs) for the portfolio optimization problem on synthetic data. Lower values are better.
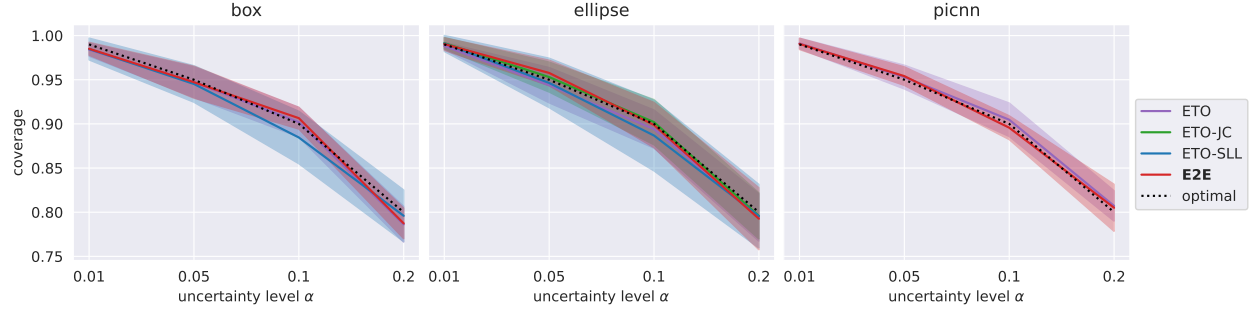

Figure 7: Coverage (mean ± 1 stddev across 10 runs) for the portfolio optimization problem on synthetic data, with the dotted black line indicating the target coverage level α.

representation, when learned end-to-end, performs better than box uncertainty and comparably with ellipse uncertainty. The similarity in performance between E2E ellipsoidal uncertainty and E2E PICNN uncertainty is likely due to the underlying aleatoric uncertainty (*i.e.,* the uncertainty in $\mathscr{P}(y \mid x)$) generally taking an ellipsoidal shape—the conditional distribution $\mathscr{P}(y \mid x)$ is still a Gaussian mixture model, and it tends to have a dominant mode. In terms of coverage, we find that all the models and training methodologies obtain coverage very close to the target level, confirming that the improvements in task loss performance from our E2E approach do not come at the cost of worse coverage.